Cement and Concrete Composites 72 (2016) 104–113

Contents lists available at ScienceDirect

Cement and Concrete Composites

journal homepage: www.elsevier.com/locate/cemconcomp

Influence of micro-cracking on the permeability of engineered cementitious composites

Hezhi Liu [a, b, c], Qian Zhang [d], Chongshi Gu [a, b, c], Huaizhi Su [a, b, c], Victor C. Li [e, *]

[a] College of Water Conservancy and Hydropower Engineering, Hohai University, Nanjing, 210098, China
[b] State Key Laboratory of Hydrology-Water Resources and Hydraulic Engineering, Hohai University, Nanjing, 210098, China
[c] National Engineering Research Center of Water Resources Efficient Utilization and Engineering Safety, Hohai University, Nanjing, 210098, China
[d] Department of Civil and Environmental Engineering, University of Louisiana at Lafayette, United States
[e] Department of Civil and Environmental Engineering, University of Michigan, Ann Arbor, MI, United States

ARTICLE INFO

Article history:
Received 3 August 2015
Received in revised form
8 April 2016
Accepted 21 May 2016
Available online 25 May 2016

Keywords:
Engineered cementitious composites (ECC)
Permeability
Multiple cracking
Measurement and model
Hydraulic structures

ABSTRACT

Engineered Cementitious Composites (ECC) forms multiple micro-cracks under tension when loaded to beyond the elastic stage. Unlike normal concrete, such tight cracks help to maintain low water permeability even in the cracked stage. Therefore ECC shows great potential for application in hydraulic structures, such as dams and levees for which water seepage control is critical for their performance. In this paper, the permeability of ECC under constant tensile load was experimentally studied using a specially designed displacement-control loading device, providing permeability data for ECC under realistic loading conditions. In addition, an analytical model capable of predicting permeability property of ECC composite based on tensile strain and crack patterns has been proposed and experimentally verified on two different ECC mixtures. The findings of this research are expected to support future design and application of ECC for hydraulic structures.

© 2016 Elsevier Ltd. All rights reserved.

1. Introduction

Seepage in concrete dams poses a great threat to the safety of the structures. Approximately one third of all dam failures are caused by seepage problem [1]. Severe seepage results in loss of water in the reservoir, and is also responsible for water infiltration into the dam that may lead to freeze-thaw and frost-heaving damage in cold regions. More importantly, the structure may lose stability when such damage happens within the dam or dam foundation [2]. One example for dam failure caused by seepage problem is the collapse of Idbar Dam in Yugoslavia in 1960. Water seepage resulted in piping and erosion of the dam foundation, which then led to the collapse of the dam during its first filling [3].

In addition to dams, seepage control is also critical to other hydraulic structures such as levees, spillways and sluices. Severe seepage increases the risk of structural failure by reducing the effective stresses exerted on the foundation of these structures that may result in a loss of support stability. Additionally, excessive pore water within concrete material may also result in piping and internal erosion, leading to damage of the structure. For example, the spillway collapse of a reservoir in Qinghai Province, China in 2005 is due to the seepage between the dam and spillway, which resulted in internal erosion of the foundation [4]. Therefore, seepage needs to be carefully controlled to ensure the safety and durability of these hydraulic structures.

Current seepage control methods include applying waterproof concrete panels/curtain grouting (with low water permeability) on the upstream side of the hydraulic structure, or installing drain pipes/drain holes on the downstream side. Among these, waterproofing concrete panels is considered one of the most effective and most commonly used methods nowadays [5,6]. However, the effectiveness of this method depends critically on the performance of the waterproofing concrete material which tends to form large cracks under structural and/or environmental loads [7,8]. As an example, Fig. 1 shows cracks formed on the upstream concrete surface of the Los Angeles Dam. Such large cracks increase the water permeability of the concrete panels under hydraulic pressure and reduce the effectiveness of the seepage control. In order to ensure desirable dam performance, the cracking of the concrete panels needs to be carefully controlled.

Extensive studies have been conducted to establish the correlation between the permeability and cracking condition of cement-

* Corresponding author.
E-mail address: vcli@umich.edu (V.C. Li).

http://dx.doi.org/10.1016/j.cemconcomp.2016.05.016
0958-9465/© 2016 Elsevier Ltd. All rights reserved.

based materials. Picandet et al. [10] reported that the major part of water flow through a water containing structure is conveyed by cracks. Wang et al. [11] found that the permeability increases slowly from uncracked condition up to crack opening of 50 μm, followed by a sharp increase of the permeability as crack width increases from 50 μm to 200 μm. Wang et al. and Tsukamoto [12] pointed out that the water permeability of concrete scales with the 3rd power of crack width when the crack width is larger than 50 μm. Shah and co-workers [13–15] also observed similar trend for cracked normal strength concrete (NSC) and high strength concrete (HSC). Based on these studies, crack width less than 200 μm, and preferably less than 50 μm, is desirable for maintaining low water permeability in hydraulic concrete structures.

Engineered Cementitious Composites (ECC), a high performance fiber reinforced cementitious composites (HPFRCC) with controlled tight crack widths, is a promising alternative to concrete for the upstream waterproof application in hydraulic structures. Unlike normal concrete, ECC shows strain-hardening behavior with high ductility under tension and bending. The tensile strain capacity of ECC ranges from 2 to 5%, which is about 200–500 times larger than that of normal concrete or conventional fiber reinforced concrete (FRC) [16–19]. More importantly, the high tensile ductility of ECC is achieved by forming multiple tight micro-cracks (typically less than 100 μm wide) instead of localized large cracks, allowing the material to accommodate large deformation (caused by mechanical, environmental loads, or uneven settlement) while maintaining low water permeability at the same time. Therefore, using ECC as upstream waterproofing material for dams seems a plausible solution to enhance the performance of seepage control [20].

Crack width development, water permeability and durability characteristics of ECC have been reviewed by van Zijl et al. [21]. The water permeability of cracked ECC has been first studied by Lepech and Li [20]. In their study, it was observed that the micro-cracks formed within ECC specimens under uniaxial tensile load were approximately 60 μm in width on average. Such tight crack width allows ECC to maintain low permeability similar to that of uncracked concrete or mortar even under high tensile strain. However, the previous experiments on permeability of ECC were conducted after unloading the specimen and the crack width used in that study was residual crack width instead of crack width under loading. In reality, the crack width of ECC under tension is generally larger (by about 15% [22]) than the residual crack width. Therefore, in the previous research, the measured permeability was not directly correlated to a specific loading condition. In order to make better correlations between the real service condition and water permeability and to obtain more conservative permeability data, it is necessary to investigate the permeability of ECC while the material is tension loaded.

Fig. 1. Large cracks formed on the upstream side concrete of the Los Angeles Dam [9].

In addition to measuring the permeability under load, it is also important to develop a reliable model for predicting and understanding the permeability property of ECC. In general, under a given tensile strain, ECC exhibits multiple cracking of varying crack widths. Previous studies (e.g. Ref. [20]) typically correlate permeability with the average crack width. However, given the non-linear relationship between permeability and crack width, this correlation may produce unconservative results. A permeability model that accounts for crack width distribution of ECC under a given tensile load or strain is needed.

In the present work, the permeability of ECC under tension was studied experimentally and analytically. The permeability behavior of two ECC mixtures under tensile load was experimentally measured using a specially designed displacement-controlled loading device. Permeability behavior of a single crack at various crack widths was also studied. Based on the crack pattern and single crack permeability behavior, an analytical model capable of predicting permeability of ECC at a given strain level has been derived and experimentally verified. The research findings documented in this paper are expected to support future design and application of ECC in hydraulic structures.

2. Experimental investigation

2.1. Materials

Two ECC mixtures were used for this experimental investigation. One is a normal ECC (denoted as N-ECC) as found in previous research [23], and the other one is a ECC mixture developed incorporating crumb rubber (CR-ECC). Both ECC mixtures consist of Type I Portland cement, fine silica sand, class F fly ash, water, high range water reducing agent (HRWRA), and poly-vinyl-alcohol (PVA) fibers. In addition to the above ingredients, CR-ECC also used crumb rubber to replace part of the silica sand. The detailed mix proportions of the two ECC mixtures are shown in Table 1. The properties of PVA fiber used in this study are listed in Table 2. Previous studies [24] suggest that ECC with crumb rubber tends to show more saturated multiple-cracking behavior with significantly tighter cracks than normal ECC. Since permeability is very sensitive to crack pattern, particularly crack width, using these two distinct ECC mixtures offer the opportunity to study the effect of different crack patterns on ECC permeability. The experimental results for these two mixtures can also be used to demonstrate the wide applicability of the proposed analytical model (Section 3.3).

The preparation of the ECC mixes follows a typical ECC mixing procedure [25]. After mixing, the fresh mixtures were cast into dogbone-shaped specimens. 31 and 34 specimens were prepared using N-ECC and CR-ECC mixtures, respectively. The detailed dimensions of the dogbone specimen are shown in Fig. 2. All specimens were covered with a plastic sheet for 24 h until demolding. Specimens for permeability characterization should be in the saturated condition, otherwise capillary absorption could significantly affect the water flow [26,27]. Therefore all specimens were immersed in water at a room temperature of 23 ± 3 °C after demolding until the age of 28 days to guarantee that they were saturated at the time when permeability tests commenced.

2.2. Experimental procedures

2.2.1. Composite tensile characterization

Uniaxial tensile tests were conducted on a set of 4 dogbone specimens (for each mixture) to characterize the tensile behavior of

Table 1
Mix proportions of N-ECC and CR-ECC (kg/m^3).

Material	Cement	Sand	Fly ash	Crumb rubber	Water	HRWRA	Fiber[a]
N-ECC	393	457	865	0	311	5	26
CR-ECC	393	343	865	53	311	5	26

[a] PVA fiber content is 2% by volume.

Table 2
Properties of PVA fiber.

Length (mm)	Diameter (μm)	Elongation (%)	Density (kg/m^3)	Young's modulus (GPa)	Nominal strength (MPa)
12	39	6	1300	42.8	1600

the ECC mixtures. The tensile tests were conducted under a displacement control at 0.5 mm/min as recommended by the Japan Society of Civil Engineers (JSCE) for direct tension testing of high performance fiber reinforced cementitious composite [28]. Two linear variable displacement transducers (LVDTs) were attached diametrically opposite to each other on each dogbone specimen (with gage length of approximately 80 mm) to measure the specimen extension. The measured tensile property was used to determine the loading conditions for permeability determination in Section 2.2.2.

2.2.2. Permeability of ECC composite under tension

To investigate the permeability behavior of ECC under realistic loading conditions, dogbone specimens were uniaxially tensioned and kept at prescribed tensile strain levels for permeability test. Depending on their tensile strain capacity, N-ECC specimens were strained to and tested for permeability at tensile strains of 0%, 0.5%, 1.0%, 1.5%, 1.8%, and 2.0%; CR-ECC specimens were loaded to and tested at strains of 0%, 0.5%, 1.0%, 1.5%, 2.0%, and 2.5%.Three specimens of each mixture were tested for each prescribed strain level.

A specially designed displacement-controlled loading device was used to tension the dogbone specimens to ensure that the prescribed strain can be kept constant during later permeability test. The loading device is mainly composed of two wedges and screws, as shown in Fig. 3. The two wedges are almost identical except for the screw holes. In Fig. 3, the screw holes in the left wedge are smooth holes with diameters slightly larger than that of the screws. These holes have no restraint on the movement of the screws in the longitudinal direction. In contrast, the right wedge has threaded screw holes, fixing the screws on the right end. In addition, there are two nuts distributed on each side to retain the screws.

The above-mentioned loading device was firstly connected to a tensile testing frame with fixed-free end grip configuration to tension the specimens, in accordance with the recommendation by van Zijl et al. [29]. As shown in Fig. 4, the wedge with smooth holes was connected to the top crosshead of the testing frame, which moved upwards at a displacement rate of 0.5 mm/min during the test, while the other wedge with threaded holes was fixed to the bottom grip of the machine and did not move during the test. Two LVDTs were mounted on each side of the specimen to measure the average displacement. This part of the test procedure is the same as the regular uniaxial tensile test procedure described in 2.2.1. When the strain of the specimen (monitored using the LVDTs) reached the designated value, the two nuts adjacent to the top wedge were immediately fastened against the edge of the wedge to restrain the specimen from relaxing and the test frame loading was aborted. Then, the wedge-loading device and the specimen were taken off the loading frame and the crack pattern (crack number and crack widths) of the specimen was observed using a microscope with a resolution of 10 μm. Such resolution is required for crack width measurements based on previous studies [29]. By following such a loading procedure, the specimens were kept at the designated strain level without unloading or closing of the cracks during permeability testing.

A falling head permeability setup adopted from the literature [13] was then added to the above assemblage, allowing testing the permeability of the specimen while it is still loaded. The permeability test setup is shown in Fig. 5. The dogbone specimen (together with the loading wedges) was placed horizontally and two plexiglas water tanks were placed above and under the specimen. Rubber seals were inserted between the plexiglas water tanks and the specimen, and four thread bars were used to clamp them in place and ensure the water-tightness. Meanwhile, the lateral sides of the specimens were coated with epoxy to enforce a one-dimensional water flow. To eliminate any leakage, all joints were sealed with plumber's putty. A standpipe was mounted on the top water tank, which was used to fill the water tanks before the test and monitor the water head drop during the permeability test.

The permeability coefficient k of the ECC specimens can be determined by Darcy's law using the recorded water head data and Equation (1):

$$k = \frac{a \cdot L}{A \cdot t_f} \ln\left(\frac{h_0}{h_f}\right) \tag{1}$$

where k denotes the permeability coefficient in m/s, a is the cross-

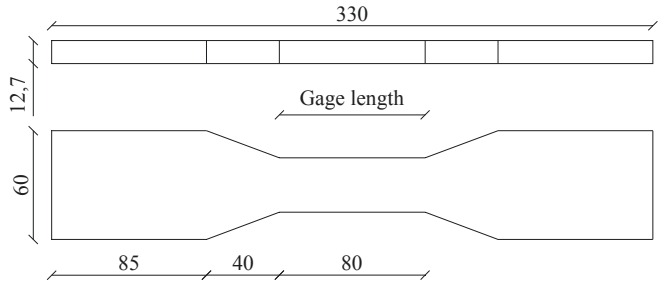

Fig. 2. Dimensions of the dogbone specimen for uniaxial tension test and permeability testing (unit: mm).

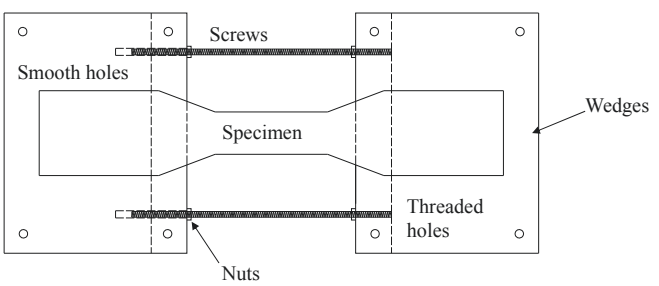

Fig. 3. Displacement-controlled loading device.

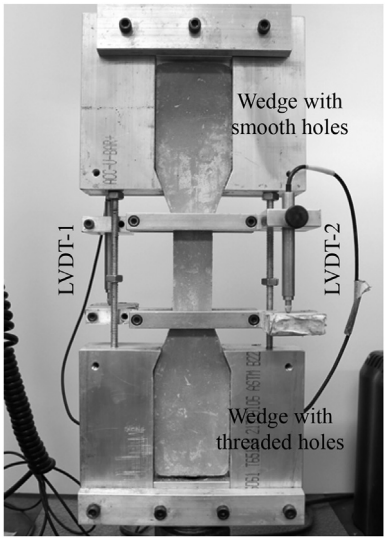

Fig. 4. Uniaxial tensile test setup.

sectional area of the standpipe (69.4 mm^2); L is the thickness of the specimen (12.7 mm); h_0 and h_f are the initial and final water head in meters, respectively; A is the cross-sectional area of the specimen subjected to water flow (2400 mm^2); and t_f is the test duration in seconds.

For this test, the water head was monitored and recorded starting at 2 h after filling the water tank. There are two considerations for choosing this measurement start time. The first one is associated with the self-healing phenomenon of ECC material. Extensive researches [30–35] have shown that ECC is able to heal the cracks by forming cement hydration products within the cracks in the presence of water. According to the references, self-healing could occur within 24 h, which significantly reduces the permeability of cracked ECC. However, in the present study, the effect of self-healing is deliberately excluded so that the permeability can be directly and distinctly correlated to the tensile strain via the measured crack pattern. To minimize the effect of self-healing, the permeability test should be conducted as soon as the specimen makes contact with water. However, in order for the Darcy's Law to be valid and to obtain meaningful result, a steady-state water flow needs to be achieved when taking the measurements. Trial permeability tests using ethanol (to suppress the self-healing phenomenon) indicate that the flow reached steady state after about 1–1.5 h. Therefore, all the permeability measurements were taken at 2 h after first filling the water tank to obtain steady-state water permeability data and to minimize the influence of self-healing.

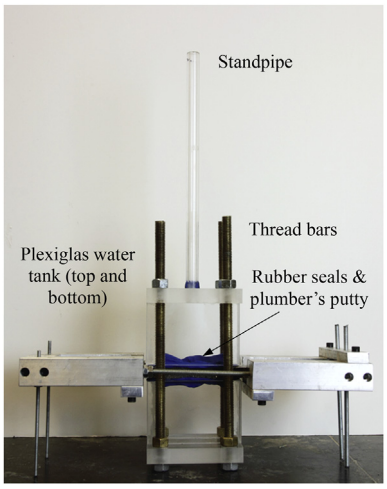

Fig. 5. Falling head permeability test setup.

2.2.3. Permeability test on specimen with single crack

To more directly correlate the permeability and crack width, the permeability test was also conducted on single crack specimens. The dogbone specimens were pre-notched (Fig. 6) in the middle to suppress the multiple cracking behavior and allow only one crack to form under tension, following the procedure suggested by Paegle and Fischer [36]. The notches are 0.5 mm wide and 5 mm deep on both sides of the specimen. In order to better control the crack width, a single crack was formed by twisting nuts on both side simultaneously instead of using the closed loop test system. Based on the maximum crack width observed during the uniaxial tensile test, these notched specimens were deformed to yield different single-crack widths ranging from 30 μm up to 100 μm for N-ECC and up to 70 μm for CR-ECC. The single crack formed on the surface in the notch region is shown in Fig. 6. It should be noted that although only a single crack was observed here, it is typically virtually impossible to cause a single crack for strain-hardening cement-based materials (such as ECC) and more than a single crack may be formed in the interior of the specimen. Three single crack specimens were tested for each crack width and each mixture.

3. Experimental results and discussion

3.1. Composite behavior

3.1.1. Tensile behavior

The measured stress-strain relationships of N-ECC and CR-ECC at 28 day are shown in Fig. 7. It is obvious that both materials achieve strain-hardening behavior with significant multiple cracking under uniaxial tensile test. N-ECC exhibits an average tensile strain capacity around 2%, and CR-ECC exhibits higher tensile strain capacity with an average of 3.5%. The tensile strength of the N-ECC and the CR-ECC is 5.3 MPa and 4.1 MPa, respectively. Such mechanical performance is considered adequate for application in hydraulic structures.

3.1.2. Crack pattern

The crack pattern of the specimens was determined based on cracks that cross a central horizontal line drawn on the specimen (Fig. 8). Crack width in multiples of 10 μm was measured using a portable microscope. The observed crack patterns, including crack number and average crack width, of N-ECC and CR-ECC at various tensile strains are shown in Table 3. As can be seen, for N-ECC and CR-ECC, both the crack width and crack number increase at the initial loading stage up to 1% strain. After this, the crack widths show little increase and the increasing strain is mainly derived from the increase in crack number. The multiple cracking behavior of ECC material with self-controlled crack width is very different from that of normal concrete, which forms only one localized crack under tension and the crack width increases indefinitely unless restrained by steel reinforcement. Formation of multiple fine cracks instead of localized large crack is expected to help ECC maintain low permeability even in the cracked stage.

It is also observed that the average crack width of CR-ECC is only about half of that of N-ECC. Since the tensile strain can be roughly estimated as the product of average crack width and crack number, larger crack number is therefore observed in CR-ECC specimens

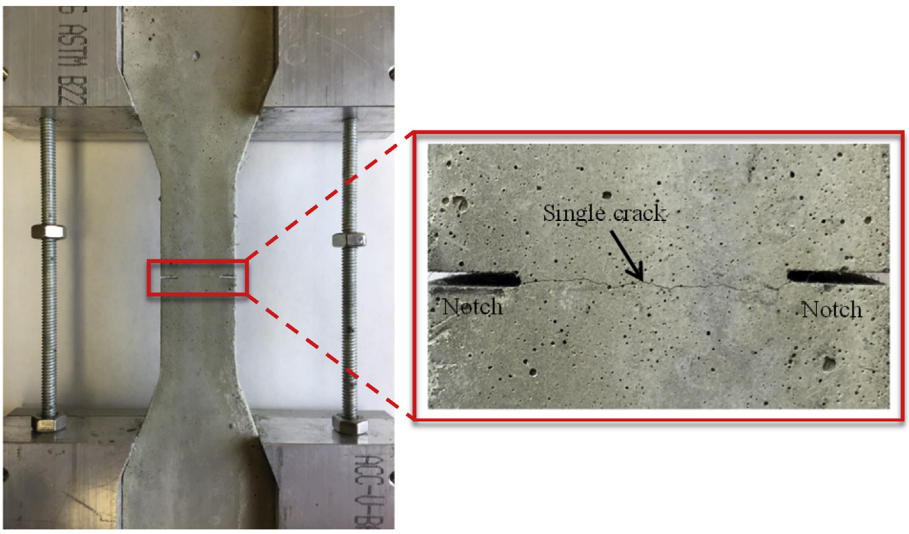

Fig. 6. Specimen for single crack permeability testing.

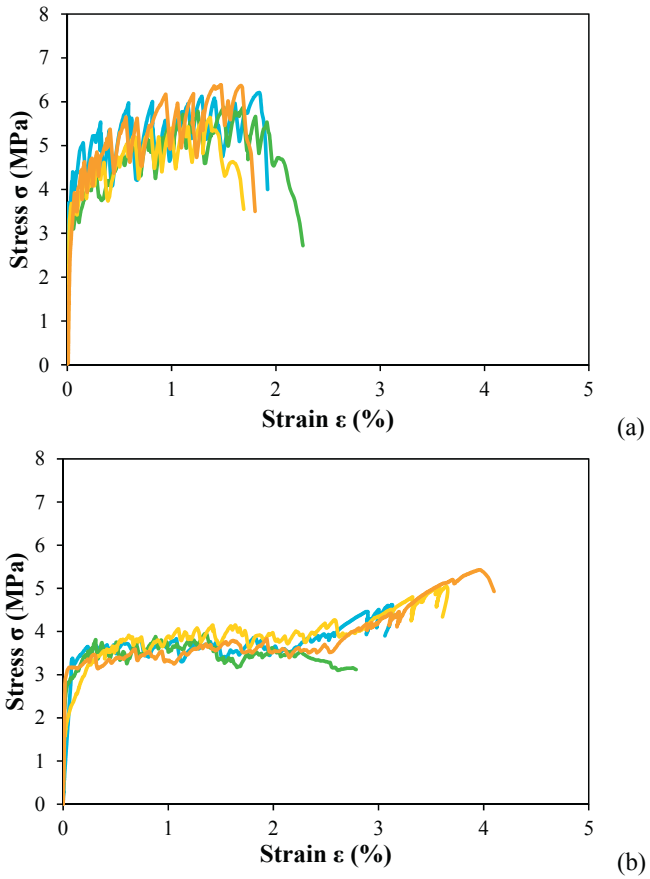

Fig. 7. Tensile stress-strain curves of (a) N-ECC and (b) CR-ECC.

than in N-ECC specimens under the same strain level. The two distinct crack patterns will also lead to different permeability behaviors of N-ECC and CR-ECC, which will be further discussed in Section 3.1.3.

As mentioned above, the product of average crack width and crack number can be used to roughly estimate the imposed strain. Based on experimental observation, the imposed strain was 20%–30% larger than the calculated values for both materials. By observing the crack pattern and the distance between the two loading-wedges before and after taking them from the testing frame, the specially designated loading device was demonstrated to effectively maintain the tensile strain in the specimen. With the possibility of strain release eliminated, the following reasons may contribute to the above-mentioned discrepancy.

First of all, the precision of crack detection is limited by the resolution of the portable microscope with a resolution of 10 μm. Cracks with width below 10 μm therefore cannot be observed accurately. The limitation of the microscope resolution may contribute to the smaller strain values calculated from the observed crack patterns, especially for that of CR-ECC whose crack width is mainly distributed below 20 μm. In order to obtain more accurate result, high resolution cameras and standard commercial digital image software recommended in the references [29,37] may be used in future studies. Even though the tight cracks with width below 10 μm cannot be captured in this study, the permeability results of ECC composites are not expected to be significantly affected by those cracks. The permeability of cracked ECC composites is mainly dominated by larger cracks (>30 μm).

Another reason that might have contributed to the discrepancy between measured and calculated imposed strain might be associated with the crack width variation along the cracks. The assumption of a constant width along the crack is only an approximation at best. Recording only the crack width crossing the horizontal lines drawn on the specimen surface may not accurately reflect the actual crack pattern. This can be improved to some extent with more measurement points along the cracks. In addition, only surface crack was monitored in this research. The crack

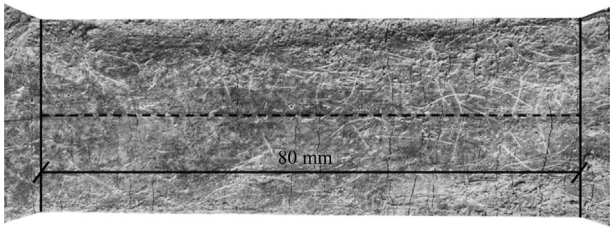

Fig. 8. Crack patterns of an N-ECC specimen at 1% strain.

Table 3
Crack pattern of N-ECC and CR-ECC under various imposed strains.

Strain (%)	Avg. crack width (μm)	Avg. no. of cracks
N-ECC		
0	0	0
0.5	33	8
1.0	48	13
1.5	53	18
1.8	54	20
2.0	55	24
CR-ECC		
0	0	0
0.5	25	11
1.0	28	22
1.5	29	32
2.0	33	36
2.5	32	48

patterns in the interior of the specimen may be different from that on the surface. X-ray computed microtomography (μCT) [38] may be used in the future for better observations.

The typical observed crack width distribution for each material at their highest investigated strain level and corresponding best-fitting lognormal distribution curves are plotted in Fig. 9. By using the best-fitting curves, the crack patterns can be mathematically expressed using the probability density function (PDF) of the fitted lognormal distribution curve. This PDF will be used in later analytical analysis in Section 3.3. Since the crack widths were observed using a microscope with a resolution of 10 μm, it is only meaningful when the crack widths are in multiples of 10 μm. However, the PDF used in this study is a continuous function of crack width for simplicity of the analytical investigation. Similarly, the best-fitting lognormal distribution curves of crack width at other strain levels are summarized and plotted in Fig. 10. From Figs. 9 and 10, it is apparent that the crack patterns are very different between these two materials. As mentioned above, the crack widths of N-ECC are greater than that of CR-ECC at all strain levels while the crack numbers show an opposite trend. The lognormal distribution of crack width in ECC has also been observed by Wang et al. [39] and Ranade et al. [37].

The PDF of the fitted lognormal distribution can be expressed as:

$$p(\delta,\varepsilon)=\frac{1}{\delta\sigma\sqrt{2\pi}}e^{\frac{-(\ln\delta-\mu)^2}{2\sigma^2}} \tag{2}$$

$$\mu=\ln\frac{m^2}{\sqrt{s^2+m^2}},\ \sigma=\sqrt{\ln\left(\frac{s^2}{m^2}+1\right)} \tag{3}$$

where p (δ,ε) is the probability of crack width δ at given tensile strain ε. σ and μ are two parameters in the PDF, and can be calculated using Equation (3). m and s are the mean and standard deviation of the crack width (based on the fitted PDF), which are also functions of tensile strain ε.

The m and s for N-ECC and CR-ECC are plotted against the tensile strain in Fig. 11. These two lognormal distribution parameters can be represented by 3rd power polynomial functions of the tensile strain (ε) (Equation (4)).

$$m=A_3\varepsilon^3+A_2\varepsilon^2+A_1\varepsilon+A_0,\ s=B_3\varepsilon^3+B_2\varepsilon^2+B_1\varepsilon+B_0 \tag{4}$$

where A_i and B_i ($i=0,1,2,3$) are constant coefficients determined by 3rd-power polynomial regression analysis. The regression equations are also presented in Fig. 11. Using Equations (2)–(4), the crack pattern for each ECC material is uniquely described for a given imposed strain.

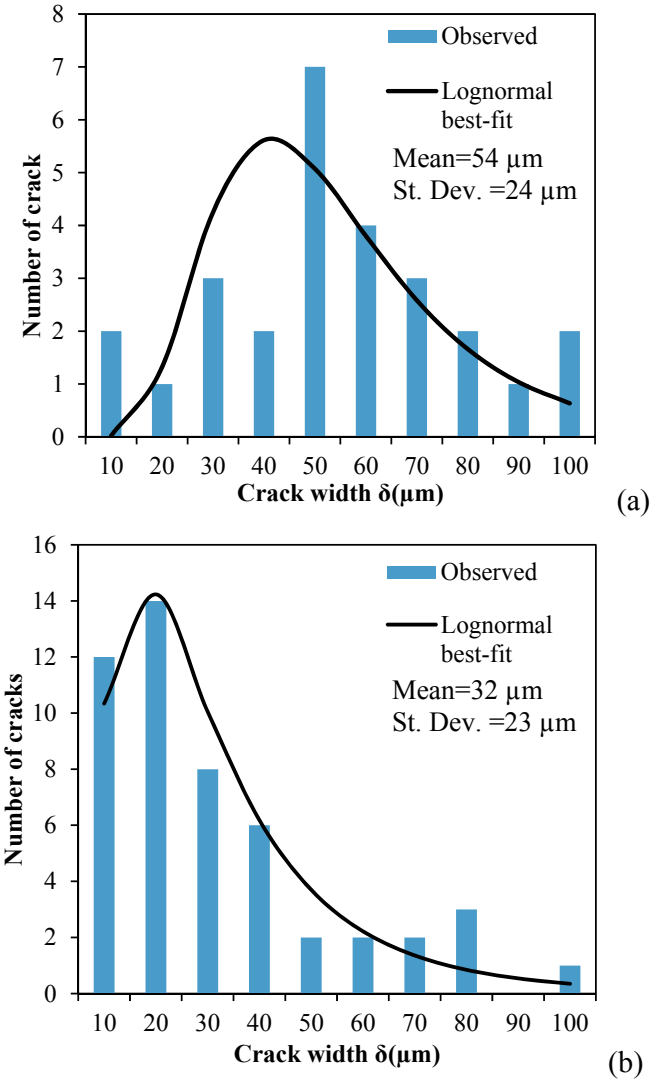

Fig. 9. Observed and best-fitting lognormal distributions for crack width distribution of (a) N-ECC, $\varepsilon = 2\%$ $\varepsilon = 2\%$ and (b) CR-ECC, $\varepsilon = 2.5\%$. $\varepsilon = 2.5\%$

3.1.3. Permeability behavior

The measured composite permeability coefficients of the two mixtures are plotted in Fig. 12 against the tensile strain. There is a clear trend of increasing permeability with increasing tensile strain for both mixtures. The permeability coefficient of N-ECC rises from 1.25×10^{-10} m/s (at 0% strain) to 2.10×10^{-7} m/s (at 2% strain). With regard to CR-ECC, the permeability coefficient increases from 2.08×10^{-10} m/s (at 0% strain) to 1.11×10^{-7} m/s (at 2.5% strain). The permeability of CR-ECC increases at a notably slower rate than that of N-ECC. In addition to the lower increasing rate, CR-ECC also shows lower average permeability compared to regular ECC at all strain levels.

The permeability performance of N-ECC and CR-ECC is closely associated with their crack patterns and especially, crack widths. In theory, the permeability of cracked material increases cubically with increasing crack width and linearly with increasing crack number [12,40,41]. Therefore, even though the crack number of CR-ECC is much higher than N-ECC, the permeability of CR-ECC is still kept lower due to its much tighter crack width. It should also be noted that despite a relatively stable average crack width under high strain levels, the standard deviations increase notably for both

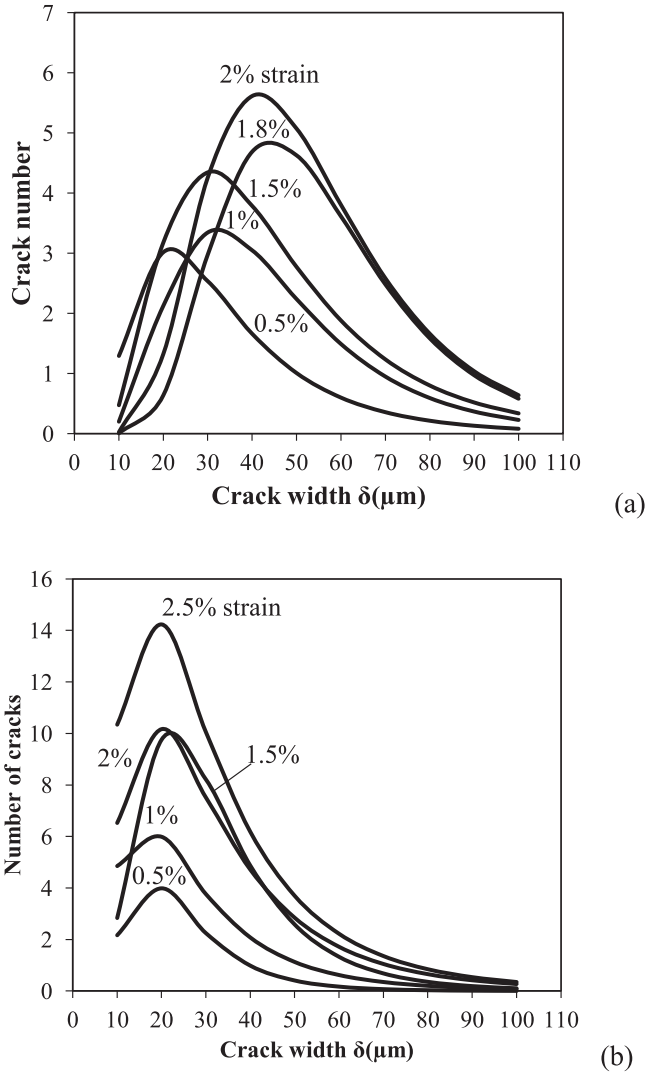

Fig. 10. Representative lognormal crack width distributions for (a) N-ECC and (b) CR-ECC, at different imposed strain values.

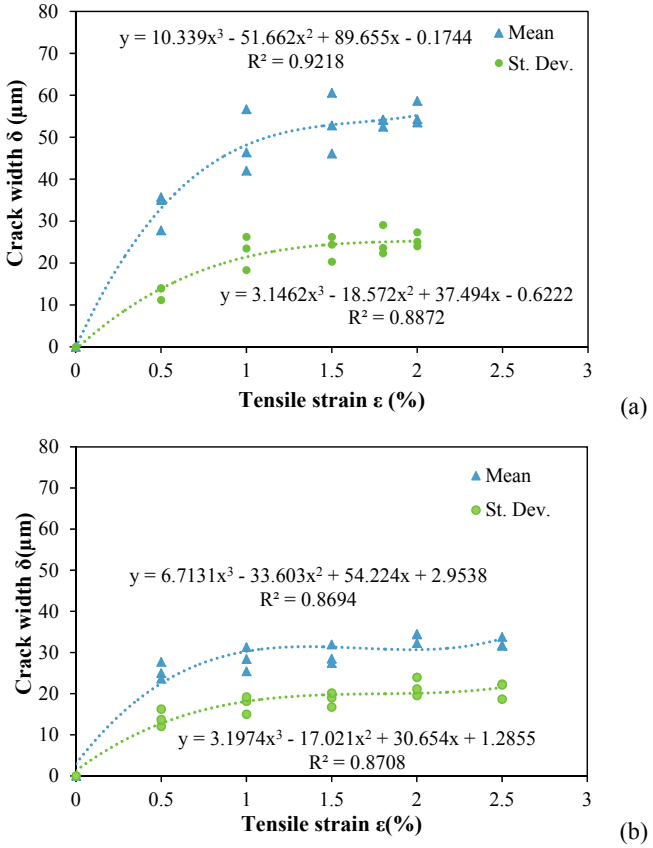

Fig. 11. Mean and standard deviation of crack width versus tensile strain for (a) N-ECC and (b) CR-ECC.

materials, resulting in a greater variation in the permeability properties at higher strain levels.

3.2. Single-crack behavior

To better correlate the permeability of cracked ECC with crack width, the permeability test was also conducted on notched dog-bone specimens with only one crack. Based on previously observed maximum crack width, the notched N-ECC specimens were deformed to yield single cracks of 30 μm, 60 μm, 80 μm, and 100 μm wide; and notched CR-ECC specimens were tensioned to form single cracks of 30 μm, 50 μm, and 70 μm wide.

The measured single crack permeability coefficients for N-ECC and CR-ECC as functions of crack width are plotted in Fig. 13. For both mixtures, the permeability increases slowly when the crack width is less than 50 μm and then increases rapidly when cracks become wider. The two sets of measured data are fitted to a single cubic function via regression analysis. The fitted curve (solid line) and corresponding equation are also presented in Fig. 13. Theoretically, the constant term of the 3rd order polynomial should be the permeability coefficient of uncracked ECC (k_0). However, the value (2.35×10^{-10} m/s) presented here was obtained via regression analysis based on the measured data for the two materials, which is quite comparable with the measured data for uncracked N-ECC and CR-ECC as mentioned above. Using this regression equation, the additional permeability induced by a single crack with given crack width can be calculated as $\Delta k(\delta) = k(\delta) - k_0$ (where k_0 is the permeability coefficient of uncracked ECC), which will be used later in Section 3.3 for predicting composite level permeability behavior. While the data in Fig. 13 were derived from two different ECCs, the resulting $k(\delta)$ is considered to be independent of the type of ECC. It captures essentially a channel flow phenomenon within the crack walls of ECC.

3.3. Analytical investigation

Now that the crack patterns ($p(\delta,\varepsilon)$) and single crack permeability behaviors ($\Delta k(\delta)$) of ECC are fully understood, it is possible to derive an analytical model to predict the composite permeability response for any ECC material with a given crack width distribution.

According to the principle of equivalent seepage resistance [41], the permeability of ECC $k(\varepsilon)$ at a given strain ε is equal to the sum of permeability of uncracked ECC (k_0) and the changes in permeability caused by cracking ($\Delta k(\varepsilon)$):

$$k(\varepsilon) = k_0 + \Delta k_c(\varepsilon_c) \tag{5}$$

The crack-induced permeability changes are further expressed as the sum of changes due to individual cracks. Suppose there are a total of $n(\varepsilon)$ cracks formed at a given tensile strain ε and the number of cracks with crack width δ_i is $n_i(\varepsilon)$. Equation (5) then becomes:

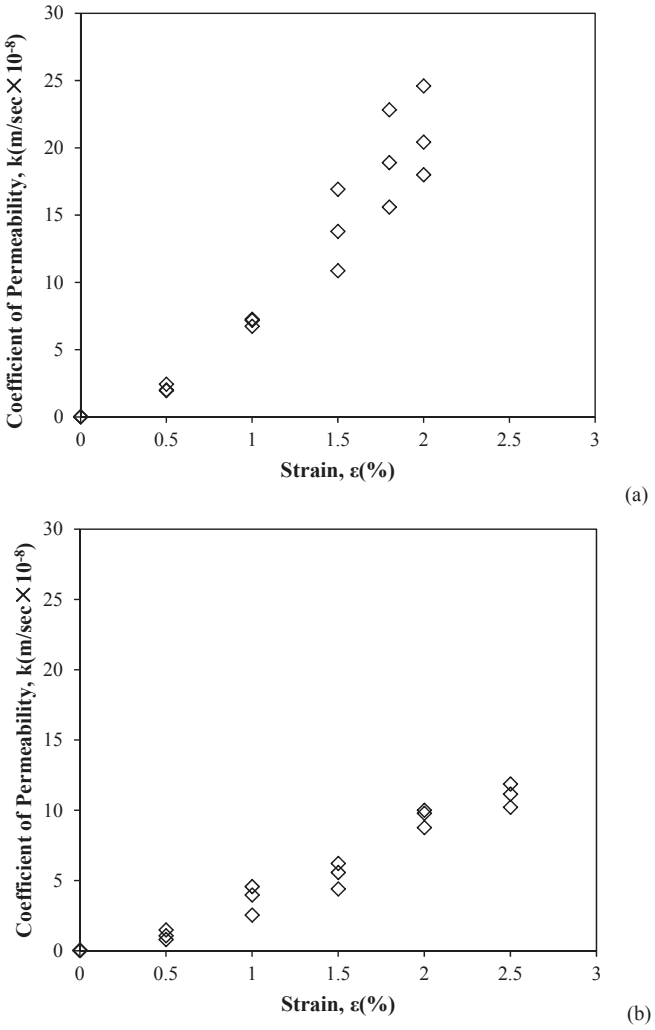

Fig. 12. Measured coefficient of permeability for (a) N-ECC and (b) CR-ECC at various strain levels.

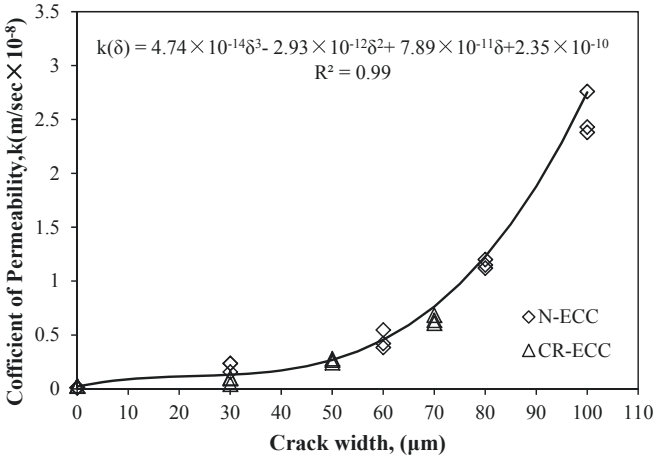

Fig. 13. Measured permeability coefficients of single-crack.

$$k(\varepsilon) = k_0 + \sum_i n_i(\varepsilon)\Delta k_i(\delta_i) \tag{6}$$

Considering the total number of cracks at a given strain ε is $n(\varepsilon)$, then $p_i(\varepsilon) = \frac{n_i(\varepsilon)}{n(\varepsilon)}$ represents the probability of a random crack with a crack width of δ_i. If a continuous PDF for crack width distribution (Equation (2)) is used, then $p_i(\varepsilon) = p(\delta_i, \varepsilon)d\delta$ and the sum becomes an integral, which means:

$$\sum_i n_i(\varepsilon)\Delta k(\delta_i) = n(\varepsilon)\int_0^\infty p(\delta,\varepsilon)\Delta k(\delta)d\delta \tag{7}$$

Then the permeability of the composite can be expressed as follow:

$$k(\varepsilon) = k_0 + n(\varepsilon)\int_0^\infty p(\delta,\varepsilon)\Delta k(\delta)d\delta \tag{8}$$

In Equation (8), the total crack number $n(\varepsilon)$ at a given strain ε can be estimated using the cracking-induced tensile displacement (caused by cracking strain ε) divided by the expected average crack width. The cracking-induced tensile displacement equals $\varepsilon_c L$, where L is the gage length. Note that the total tensile strain ε equals the sum of elastic strain ε_e and cracking strain ε, i.e. $\varepsilon = \varepsilon_e + \varepsilon_c$. Since ε_e is much smaller than ε_χ, therefore $\varepsilon_c \approx \varepsilon$. In addition, the expected average crack width is given by $\delta_{avg} = \int_0^\infty p(\delta,\varepsilon)\delta d\delta$. Hence, the total crack number $n(\varepsilon)$ is estimated to be:

$$n(\varepsilon) = \frac{\varepsilon L}{\int_0^\infty p(\delta,\varepsilon)\delta d\delta} \tag{9}$$

Then Equation (8) can be re-formulated as:

$$k(\varepsilon) = k_0 + \varepsilon L\frac{\int_0^\infty p(\delta,\varepsilon)\Delta k(\delta)d\delta}{\int_0^\infty p(\delta,\varepsilon)\delta d\delta} \tag{10}$$

Equation (10) can be used to predict the permeability coefficient of ECC composite at any tensile strain ε, given that the PDF of crack width distribution is known. The above formulation of composite permeability in terms of crack distribution pattern and single crack permeability parallels that of the formulation of composite electrical resistivity in terms of crack distribution pattern and single crack electrical resistivity [37].

In order to verify this analytical model, the model predicted permeability coefficients of N-ECC and CR-ECC at various tensile strains are plotted together with the experimental data in Fig. 14. It can be seen that the model predictions generally agree well with the experimental data, especially at lower tensile strains (<1% strain). At higher strain levels, the analytical model predicts higher permeability than the actual experimental observation. However, the predicted permeability is on the conservative side, which is desirable for safety considerations.

Several possible reasons may cause the deviation between the model prediction and the experimental data. First of all, in the model, a continuous lognormal distribution of crack width from 0 to ∞ is assumed. However, in reality, the cracks are all less than 70–100 μm. By including the nonexistent large cracks, despite the low probability, the analytical model prediction falls to the higher side than the true value. In future study, to better capture this phenomenon, a truncated lognormal distribution might be used. Another reason might be associated with the errors of the observed crack pattern as mentioned in Section 3.1.2. The failure to capture cracks below 10 μm will shift the $p(\delta,\varepsilon)$ relationship towards higher crack width space in Fig. 10. Moreover, since permeability is very sensitive to crack width, ignoring crack width variation along the

individual crack will lead to errors in $\Delta k(\delta)$ relationship when deriving the single crack permeability behavior. Such error can be eliminated to some extent with more careful observation of the crack pattern. Finally, in spite of careful cutting of the notch to produce the "single crack", it is plausible that more than a single crack is formed in the interior of the specimen due to the intrinsic strain-hardening nature of ECC, which would lead to a higher measure Δk (δ) and a computed $k(\varepsilon)$. Despite all this, the model predictions capture the data trends and err on the conservative side.

Based on both experimental observations and the analytical model, the permeability of ECC material can be estimated as a quadratic function of the tensile strain. The regression equations of the experimental data are shown in Fig. 14. For normal concrete with localized cracks, the tensile strain of cracked concrete is mainly attributed to widening of the cracks. Therefore, the permeability of cracked concrete is a cubic function of the strain (crack width control). Unlike normal concrete, ECC develops multiple micro-cracks when subjected to tensile loading. The tensile strain increase is associated with both crack number increase and crack width increase. Therefore the relationship between the permeability of cracked ECC and tensile strain should be bounded between a linear relationship (controlled by crack number) and a cubic relationship (controlled by crack width). According to the research findings in this paper, a quadratic function can be used to estimate the permeability-tensile strain relationship of ECC with acceptable accuracy. This also explains the reason that ECC shows much lower permeability under tensile load compared to normal concrete.

4. Conclusions

The influences of micro-cracks on the composite permeability response of ECC under tension were experimentally explored and an analytical model for predicting the permeability of ECC composite was proposed and verified in this paper. Based on the research findings, the following conclusions can be drawn:

1. The specially designed loading device described in this paper is effective in measuring the permeability of cracked ECC while under load, providing more accurate and realistic permeability data.
2. The permeability of cracked ECC is closely associated with crack pattern in general and crack width in particular. CR-ECC with tighter crack width exhibits significantly lower permeability than N-ECC under the same imposed tensile strain, despite a higher permeability value in the uncracked state. This speaks to the importance of self-control of crack width.
3. An analytical model for predicting the permeability of ECC composite based on crack width distribution and single crack permeability behavior has been proposed and experimentally verified. The model prediction is acceptably accurate and on the conservative side.
4. Unlike normal concrete, the permeability of cracked ECC can be estimated as a quadratic function of the tensile strain, which explains the lower permeability of ECC under cracked stage compared to normal concrete, the permeability of which scales with the third power of the localized crack width.

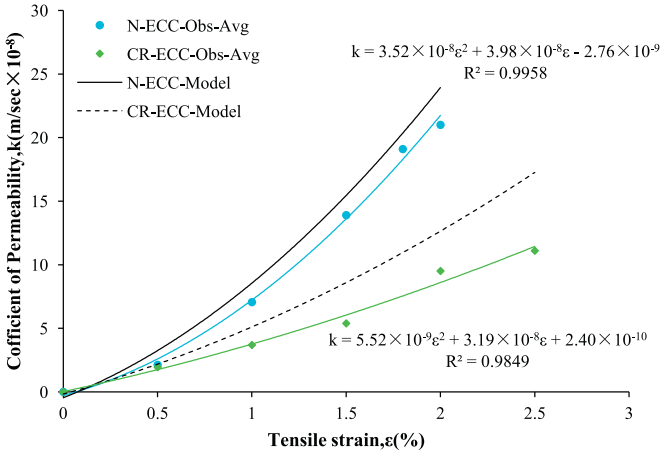

Fig. 14. Modeled and observed permeability behavior of N-ECC and CR-ECC.

The experimental data and derived analytical model presented in this paper can be used to study the behavior of cracked ECC in the strain-hardening stage and provide guidelines for future application of ECC in hydraulic structure. Specifically, the permeability of hydraulic infrastructure can be predicted once the distributed strain is known (e.g. via finite element calculation), and if the crack pattern for the ECC used is characterized experimentally. In future study, to more accurately simulate the real service condition, consideration of self-healing phenomenon of ECC can also be incorporated into the model.

Acknowledgements

This research was partially funded by National Natural Science Foundation of China (Grant Nos.51139001, 51479054, 51579085, 51279052), Priority Academic Program Development of Jiangsu Higher Education Institutions (Grant No. YS11001), Open Foundation of State Key Laboratory of Hydrology-Water Resources and Hydraulic Engineering (SN: 20145027612), Research Fund for the Doctoral Program of Higher Education of China (Grant Nos.20120094130003, 20130094110010), Jiangsu Province "Six Talent Peaks" Project (Grant Nos. JY-008, JY-003), China Scholarship Council (CSC), and the China Thousand Talent Program. This research was performed at the University of Michigan while H. Liu served as a visiting scholar.

References

[1] J. Chai, S. Li, Analysis of seepage through dam foundation with closed system of grouting curtain, drainage and pumping measures, in: Proceedings of the 4th International Conference on Dam Engineering. Tan, Nanjing, China, 2004, pp. 171–176.
[2] H.R. Cedergren, Seepage, Drainage, and Flow Nets, John Wiley & Sons, 1997.
[3] F.E.R. Commission, Engineering Guidelines for the Evaluation of Hydropower Projects, 1999, pp. 11–18 (Chapter 11)-Arch Dams, Washington DC 20426.
[4] Y. Xiang, F. Ma, H. Yuan, Cause analysis of the spillway collapse of a reservoir, Water Power 33 (6) (2007) 89–92.
[5] C. Shen, S. Wang, Y. Lin, X. Liu, Hydraulic Strictures, China Waterpower Press, 2008.
[6] Y. Zhu, X. Chu, Practice in seepage prevention structures of roller-compacted concrete dams, J. Hohai Univ. Nat. Sci. 31 (1) (2003) 16–20.
[7] P. Rossi, F. Toutlemonde, Effect of loading rate on the tensile behaviour of concrete: description of the physical mechanisms, Mater. Struct. 29 (2) (1996) 116–118.
[8] K. Wang, D.E. Nelsen, W.A. Nixon, Damaging effects of deicing chemicals on concrete materials, Cem. Concr. Compos. 28 (2) (2006) 173–188.
[9] R.A. Page, D.M. Boore, R.F. Yerkes, The Los Angeles Dam Story, US Geological Survey, 1995.
[10] V. Picandet, A. Khelidj, H. Bellegou, Crack effects on gas and water permeability of concretes, Cem. Concr. Res. 39 (6) (2009) 537–547.
[11] K. Wang, D.C. Jansen, S.P. Shah, A.F. Karr, Permeability study of cracked concrete, Cem. Concr. Res. 27 (3) (1997) 381–393.
[12] M. Tsukamoto, Tightness of fiber concrete, Darmstadt Concr. 5 (3) (1990) 215–225.
[13] C.-M. Aldea, M. Ghandehari, S.P. Shah, A. Karr, Estimation of water flow through cracked concrete under load, ACI Mater. J. 97 (5) (2000).
[14] C.-M. Aldea, S.P. Shah, A. Karr, Effect of cracking on water and chloride permeability of concrete, J. Mater. Civ. Eng. 11 (3) (1999) 181–187.

[15] C.-M. Aldea, S. Shah, A. Karr, Permeability of cracked concrete, Mater. Struct. 32 (5) (1999) 370–376.
[16] V.C. Li, Advances in ECC Research, ACI Special Publication on Concrete: Material Science to Applications SP 206-23, 2002, pp. 373–400.
[17] V.C. Li, On engineered cementitious composites (ECC) a review of the material and its applications, J. Adv. Concr. Technol. 1 (2003) 215–230.
[18] V.C. Li, Engineered cementitious composites (ECC)–tailored composites through micromechanical modeling, in: N. Banthia, A. Bentur, A. Mufti (Eds.), Fiber Reinforeced Concrete:present and the Future, Canadian Society for Civil Engineering, Montreal, 1998, pp. 64–97.
[19] M.B. Weimann, V.C. Li, Drying shrinkage and crack width of ECC, in: A.M. Brandt, V.C. Li, I.H. Marshall (Eds.), Proc. Of the Seventh Int'l Symp. on Brittle Matrix Composites (BMC-7), Warsaw, Poland, 2003, pp. 37–46.
[20] M.D. Lepech, V.C. Li, Water permeability of engineered cementitious composites, Cem. Concr. Compos. 31 (10) (2009) 744–753.
[21] G.P. van Zijl, F.H. Wittmann, B.H. Oh, P. Kabele, R.D. Toledo Filho, E.M. Fairbairn, V. Slowik, A. Ogawa, H. Hoshiro, V. Mechtcherine, Durability of strain-hardening cement-based composites (SHCC), Mater. Struct. 45 (10) (2012) 1447–1463.
[22] Y. Yang, M.D. Lepech, E.-H. Yang, V.C. Li, Autogenous healing of engineered cementitious composites under wet–dry cycles, Cem. Concr. Res. 39 (5) (2009) 382–390.
[23] Z. Zhang, S. Qian, H. Ma, Investigating mechanical properties and self-healing behavior of micro-cracked ECC with different volume of fly ash, Constr. Build. Mater. 52 (2014) 17–23.
[24] Z. Zhang, H. Ma, S. Qian, Investigation on properties of ECC incorporating crumb rubber of different sizes, J. Adv. Concr. Technol. 13 (5) (2015) 241–251.
[25] X. Huang, R. Ranade, V.C. Li, Feasibility study of developing green ECC using iron ore tailings powder as cement replacement, J. Mater. Civ. Eng. 25 (7) (2012) 923–931.
[26] P. Zhang, F. Wittmann, T. Zhao, E. Lehmann, L. Tian, P. Vontobel, Observation and quantification of water penetration into Strain Hardening Cement-based Composites (SHCC) with multiple cracks by means of neutron radiography, Nucl. Instrum. Methods Phys. Res. Sect. A Accel. Spectrom. Detect. Assoc. Equip. 620 (2) (2010) 414–420.
[27] C. Schröfl, V. Mechtcherine, A. Kaestner, P. Vontobel, J. Hovind, E. Lehmann, Transport of water through strain-hardening cement-based composite (SHCC) applied on top of cracked reinforced concrete slabs with and without hydrophobization of cracks–Investigation by neutron radiography, Constr. Build. Mater. 76 (2015) 70–86.
[28] J.C. Committee, Recommendations for design and construction of high performance fiber reinforced cement composites with multiple fine cracks, in: K. Rokugo (Ed.), Japan Society of Civil Engineers, Tokyo, Japan, 2008.
[29] G.P. van Zijl, V. Slowik, R.D. Toledo Filho, F.H. Wittmann, H. Mihashi, Comparative testing of crack formation in strain-hardening cement-based composites (SHCC), Mater. Struct. 1–15.
[30] V.C. Li, E.N. Herbert, Self-healing of microcracks in engineered cementitious composites (ECC) under a natural environment, Materials 6 (2013) 2831–2845.
[31] L.L. Kan, H.S. Shi, A.R. Sakulich, V.C. Li, Self-healing characterization of engineered cementitious composite materials, ACI Mater. J. 107 (2010) 617–624.
[32] M. Wu, B. Johannesson, M. Geiker, A review: self-healing in cementitious materials and engineered cementitious composite as a self-healing material, Constr. Build. Mater. 28 (1) (2012) 571–583.
[33] K. Van Tittelboom, N. De Belie, D. Van Loo, P. Jacobs, Self-healing efficiency of cementitious materials containing tubular capsules filled with healing agent, Cem. Concr. Compos. 33 (4) (2011) 497–505.
[34] A. Hosoda, T. Kishi, H. Arita, Y. Takakuwa, Self healing of crack and water permeability of expansive concrete, in: 1st International Conference on Self-healing Materials, 2007, pp. 18–20.
[35] M. Li, V.C. Li, Cracking and healing of engineered cementitious composites under chloride environment, ACI Mater. J. 108 (2011) 333–340.
[36] I. Paegle, G. Fischer, Evaluation of standardized test methods to characterize fiber reinforced cement composites, in: R. Toledo Filho, F. Silva, E. Koenders, E. Fairbairn (Eds.), SHCC2, RILEM Publications SARL, Rio de Janeiro, Brazil, 2011, pp. 9–16.
[37] R. Ranade, J. Zhang, J.P. Lynch, V.C. Li, Influence of micro-cracking on the composite resistivity of engineered cementitious composites, Cem. Concr. Res. 58 (2014) 1–12.
[38] S. Fan, M. Li, X-ray computed microtomography of three-dimensional microcracks and self-healing in engineered cementitious composites, Smart Mater. Struct. 24 (1) (2014) 015021.
[39] P. Wang, F. Wittmann, T. Zhao, W. Huang, R. Toledo Filho, F. Silva, E. Koenders, E. Fairbairn, Evolution of crack patterns on shcc as function of imposed strain, in: 2nd International RILEM Conference on Strain Hardening Cementitious Composites (SHCC2-Rio), RILEM Publications SARL, 2011, pp. 217–224.
[40] T. Yu, L. Wei-qun, An equivalent seepage resistance model with seepage-stress coupling for fractured rock mass, Rock Soil Mech. 33 (7) (2012) 2041–2047.
[41] A.M. Gal'perin, Hydrogeology and Engineering Geology: Geotechnika-selected Translations of Russian Geotechnical Literature 8, CRC Press, 1993.